Developing a new near-real time fire emissions product from VIIRS daily global coverage

Niels Andela*[1], Douglas C. Morton[1], Guido R. van der Werf[2], Wilfrid Schroeder[3], Louis Giglio[4], Yang Chen[5], and James T. Randerson[5]

*niels.andela@nasa.gov, [1]NASA Goddard Space Flight Center, [2]VU University Amsterdam, [3]NOAA, [4]University of Maryland College Park, [5]University of California Irvine.

Abstract

Biomass burning on natural and agricultural lands has profound effects on atmospheric chemistry, climate, and air quality. Over the past decade, a number of global fire emissions inventories have been developed based on near real-time detection of actively burning fires by the MODIS instruments. However, the MODIS instruments provide variable and incomplete global sampling of fire activity, resulting in large uncertainty in the spatiotemporal accuracy of emissions inventories. Here, we compared active fire products from MODIS and VIIRS to characterize product-specific shortcomings of each system with the goal to develop a new, more accurate, global emissions inventory. For the development of our near real-time emissions product, we used the VIIRS 375m product (VNP14IMGML) that detected most FRP and retained best sensitivity across the swath, starting in 2012. From 2019 onwards we combined observations from both VIIRS instruments onboard NOAA20 and SNPP, that together provide improved daily global near-nadir coverage. Finally, we used regional conversion factors to create a near real-time emissions inventory that is consistent with long-term patterns of biomass burning from the Global Fire Emissions Database (GFED) 4s.

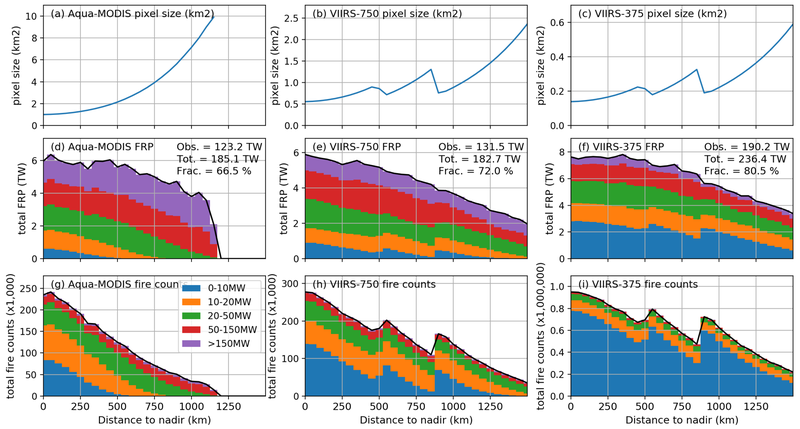

Figure 1: Global sum of fire radiative power (FRP) and fire counts during 2018 as a function of distance to nadir. Increasing pixel area and atmospheric path reduce the sensitivity of all instruments and products at greater distance to nadir, in addition, MODIS does not provide global daily coverage at the equator.

Correction for view geometry

Based on the VIIRS 375m product, we explored two strategies to correct for the loss of sensitivity to low FRP fires at greater observational angles. The first strategy estimates regional correction factors based on total FRP observed at different distance to nadir (Fig. 2). The second strategy exists of a set of global correction factors that depend on the observed FRP and distance to nadir (Fig. 3).

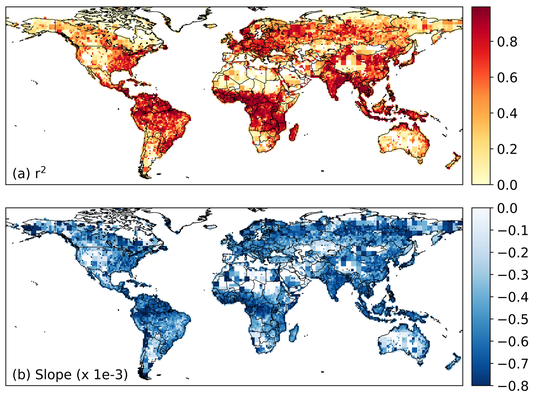

Figure 2: Regional correction factors to account for loss in sensitivity to FRP at larger observation angles. (a) correlation between distance to nadir and total observed FRP (2012-2018). (b) slope between normalized FRP observed at nadir and distance to nadir used to create a correction factor. Strongest correlation and largest correction factors occur across regions characterized by low-FRP fires.

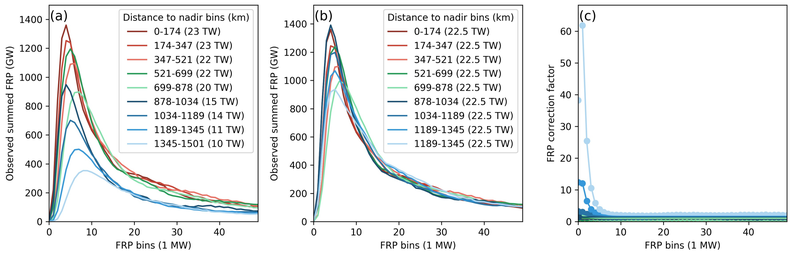

Figure 3: Global correction factors depending on FRP and distance to nadir. (a) observed FRP, (b) corrected FRP, and (c) correction factor.

Corrected FRP and emissions estimates

We compared corrected FRP estimates from SNPP-VIIRS only to combined near-nadir observations from the two VIIRS instruments onboard NOAA20 and SNPP starting in 2019. Correction factors effectively filled in most of the global (Fig. 4) and regional (Fig. 5) "missed" FRP. Large differences in spatial patterns of emissions estimates from GFED4s.NRT (developed here) and GFASv1.2 highlight the importance of accurate regional estimates of total FRP (Fig. 6). While the added FRP reduced day-to-day variability in observed FRP driven by the instrument's position, the (sometimes large) correction factors also increased the spatiotemporal uncertainty through added noise. We compared day-to-day correlation between FRP and NO_2 (OMI), a short lived trace gas, to understand how well corrected daily FRP time series captured day-to-day variability in fire emissions. We decided to use the corrected FRP time series based on regional correction factors, that retained overall daily performance, in contrast to the global correction factors that reduced correlation coefficients. In both instances, correlation coefficients with daily NO_2 further improved when using a running-mean (Fig. 7).

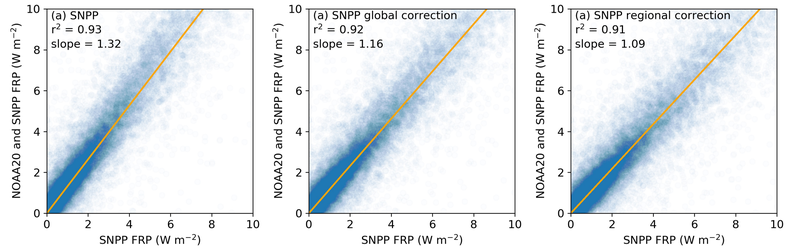

Figure 4: Spatial correlation and slope between corrected FRP from SNPP-VIIRS only and near-nadir observations from the combination of NOAA20 and SNPP VIIRS (Global, Apr. to Oct. 2019). (a) SNPP VIIRS, (b) SNPP VIIRS using the global correction factor, and (c) SNPP VIIRS using the regional correction factor.

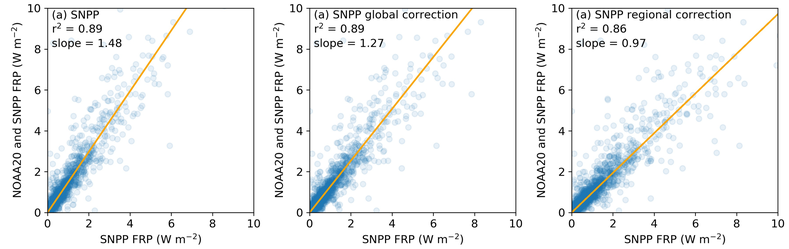

Figure 5: Spatial correlation and slope between corrected FRP from SNPP-VIIRS only and near-nadir observations from the combination of NOAA20 and SNPP VIIRS for India, a small (low FRP) fire region (Apr. to Oct. 2019). (a) SNPP VIIRS, (b) SNPP VIIRS using the global correction factor, and (c) SNPP VIIRS using the regional correction factor. The correction factor depends on the regional distribution of FRP values, with larger correction required in regions dominated by small (low FRP) fires.

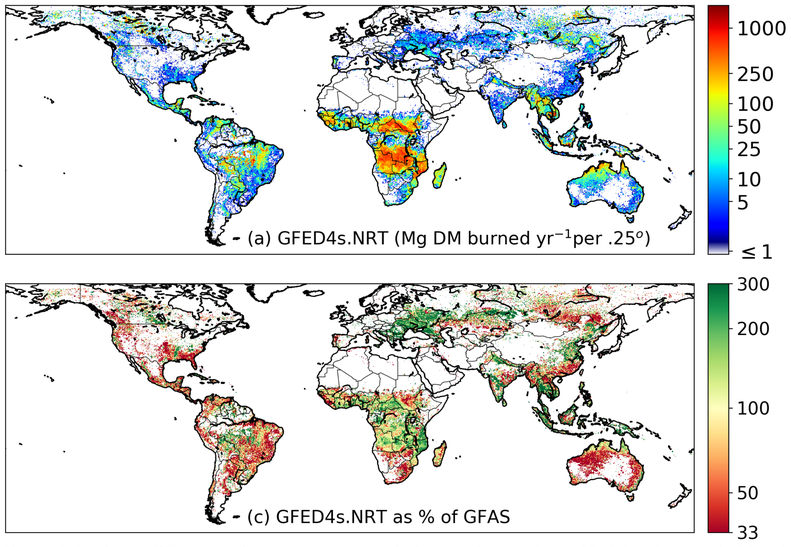

Figure 6: Regional differences in mean annual emissions estimates from GFED4s.NRT and GFASv1.2 highlight model shortcomings and consequences of regional emissions redistribution based on FRP (2013-2018). (a) Mean annual dry matter burned estimated by GFED4s.NRT. (b) Mean annual GFED4s.NRT CO_2 emissions as fraction of GFASv1.2 emissions estimates.

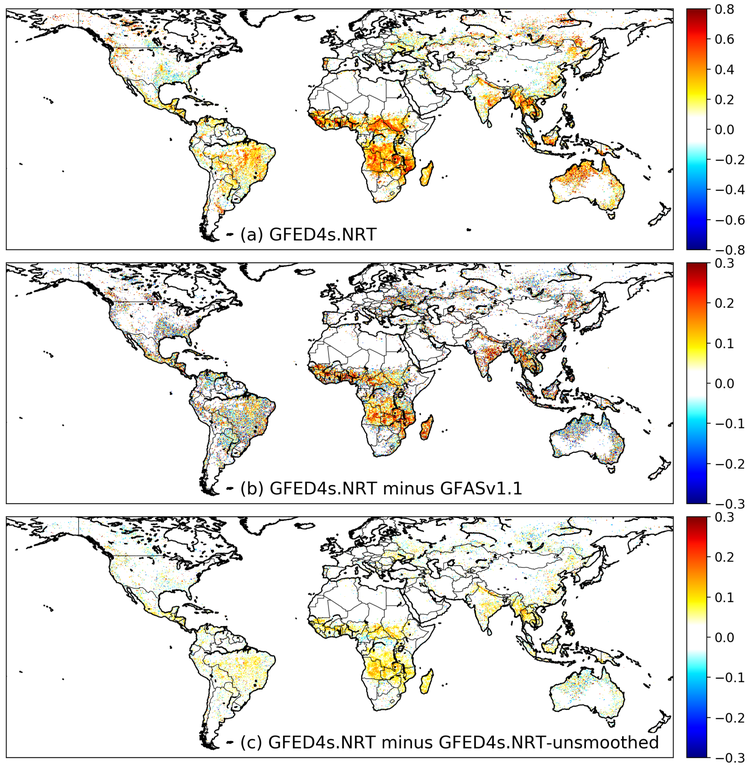

Figure 7: Correlation coefficients between daily estimated NO_2 emissions and observed column NO_2 from OMI (2013 – 2018). (a) Correlation between GFED4s.NRT and OMI NO_2 for all days with a per-grid cell FRP of ≥100 MW and cloud free OMI overpass. (b) Difference in correlation coefficients based on NO_2 estimates from GFED4s.NRT and GFAS1.2 compared to OMI NO_2. (c) Difference in correlation coefficients based on smoothed (running mean) and unsmoothed GFED4s.NRT emissions estimates compared to OMI NO2.

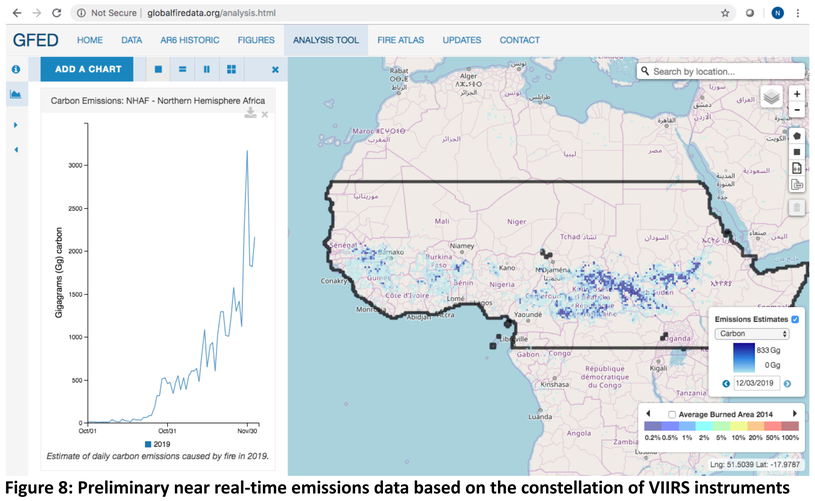

Figure 8: Preliminary near real-time emissions data based on the constellation of VIIRS instruments onboard NOAA20 and SNPP can be explored online at www.globalfiredata.org (starting in 2019).

Conclusions

1. After correction, the VIIRS 375m (VNP14IMGML) time series result in nearly double the observed FRP compared to uncorrected data from Aqua MODIS (both 1:30 pm overpasses). Differences in spatial patterns highlight large scale underestimates of fire radiative power from often densely populated small fire regions based on older sensors (MODIS) and/or uncorrected data.
2. The SNPP VIIRS-based emissions estimates are more consistent with daily NO_2 observations from OMI compared to MODIS based emissions estimates (i.e. GFAS). Nevertheless, correlation coefficients further improve when using a running-mean, indicating considerable residual day to day variability in FRP detections not related to variation in fire activity.
3. Starting in 2019, the combined VIIRS instruments onboard NOAA20 and SNPP provide better global near-nadir coverage, improving the spatial-temporal accuracy of emissions estimates.